

Qubit-efficient encoding schemes for binary optimisation problems

Benjamin Tan^{1,*}, Marc-Antoine Lemonde^{1,†}, Supanut Thanasilp¹,

Jirawat Tangpanitanon¹, and Dimitris G. Angelakis^{1,2‡}

¹ *Centre for Quantum Technologies, National University of Singapore, 3 Science Drive 2, Singapore 117543 and*

² *School of Electrical and Computer Engineering,
Technical University of Crete, Chania, Greece 73100*

(Dated: November 29, 2021)

We propose and analyze a set of variational quantum algorithms for solving quadratic unconstrained binary optimization problems where a problem consisting of n_c classical variables can be implemented on $\mathcal{O}(\log n_c)$ number of qubits. The underlying encoding scheme allows for a systematic increase in correlations among the classical variables captured by a variational quantum state by progressively increasing the number of qubits involved. We first examine the simplest limit where all correlations are neglected, i.e. when the quantum state can only describe statistically independent classical variables. We apply this minimal encoding to find approximate solutions of a general problem instance comprised of 64 classical variables using 7 qubits. Next, we show how two-body correlations between the classical variables can be incorporated in the variational quantum state and how it can improve the quality of the approximate solutions. We give an example by solving a 42-variable Max-Cut problem using only 8 qubits where we exploit the specific topology of the problem. We analyze whether these cases can be optimized efficiently given the limited resources available in state-of-the-art quantum platforms. Lastly, we present the general framework for extending the expressibility of the probability distribution to any multi-body correlations.

I. INTRODUCTION

In recent years, important experimental breakthroughs have propelled quantum computing as one of the most thriving fields of research [1–6], with the long-term goal of building universal quantum computers capable of running algorithms with provable quantum speed-up [7, 8]. As the first generations of quantum hardware, referred to as noisy intermediate-scale quantum (NISQ) devices [9], do not yet fulfill the technical requirements to implement error-corrected universal quantum computing, increasing efforts are dedicated to design near-term algorithms capable of performing computational tasks with imperfect and limited quantum resources [10, 11]. Amongst the most promising paradigms are the variational quantum algorithms (VQA) [12–16]. In these algorithms, a parameterized quantum circuit is optimized using classical computing resources to generate a quantum state that represents an accurate approximate solution of the problem at hand. While a formal proof of any quantum advantages these algorithms might bring has yet to be found [17], applications of NISQ devices to real-world problems are already being explored.

For instance, VQAs such as the quantum approximate optimization algorithm (QAOA) [12, 18–26] and hardware efficient [27, 28] approaches have been applied to find approximate solutions to NP-hard quadratic unconstrained binary optimisation (QUBO) problems [29]. QAOA in particular is able to ensure a lower bound on

the quality of its solutions for sparse instances of QUBO problems using shallow circuits. This quality is then able to monotonically converge towards the exact solution for infinitely deep circuits [12, 30]. Recent experiments have however highlighted the challenges in implementing the QAOA on problem graphs that differ from the native connectivity of the quantum hardware, even for small system sizes [26]. Hardware efficient approaches, on the other hand, are motivated by the simplicity of their implementations but do not guarantee a lower bound on the quality of the solutions. This is usually accomplished using series of gates native to the quantum platform and is unconstrained by the topology of the QUBO problem. However, depending on the implementation, these hardware efficient approaches can be plagued by exponentially large barren plateaus in their optimization landscapes as the number of qubits increases [31]. These barren plateaus hinder the ability to optimize these circuits efficiently and threaten to limit the number of qubits involved.

The challenges that come when employing an increasing number of qubits do not end here. While having finite coherence times and imperfect gate fidelities remain an issue, the engineering overhead of scaling up the quantum hardware currently limits the size of computational tasks to toy models. Previously proposed schemes to implement quantum algorithms to solve optimization problems have used a number of classical variables equal to the number of qubits available and were therefore limited to problem sizes involving only a few tens of them [20–28]. This is not representative of real-world optimization problems, where the number of classical variables n_c involved are often on the order of 10^4 . In order to test the performance of NISQ devices on more realistic optimization problems, alternative methods of encoding the

*b.tan@u.nus.edu

†cqtml@nus.edu.sg

‡dimitris.angelakis@qubit.org

classical variables onto the limited number of qubits are required.

In this work, we tackle this problem by proposing a hardware efficient encoding scheme for QUBO models with n_c variables that can be implemented on $\mathcal{O}(\log n_c)$ number of qubits. In this context, a variational quantum state encodes a probability distribution over all classical solutions and the variational process aims at producing a state with maximal probability associated with the best solutions. We show that by dividing the total number of qubits $n_q = n_a + n_r$ into a group of n_a ancillas and a group of n_r register qubits, one can in principle use this probability distribution to encode any n_a -body correlations between a number of QUBO variables that scale exponentially with n_r . This heuristic approach allows for the systematic increase in the correlations that can be captured in the probability distribution by progressively increasing the number of qubits.

As an example, in the limit where all correlations are neglected, $n_r = \log_2(n_c)$ and optimization problems of $n_c \sim 10^4$ classical variables could be tackled on quantum hardware with no more than 15 qubits. We present a variational approach based on this minimal encoding and investigate its performance for increasing problem sizes. From there, we consider protocols to encode different subsets of two-body correlations and explore whether they can be optimized efficiently. We demonstrate how a selective encoding scheme can be applied to the Max-Cut problem, a sparse instance of QUBO models, and show that exploiting the topology of a specific problem to select an efficient subset of correlations leads to better solutions. All protocols proposed in this manuscript are in line with the limitations of the current state-of-the-art quantum platforms. These alternative encoding schemes could pave the way towards NISQ devices having practical applications with performances comparable to classical algorithms when it comes to large-scale optimization problems.

II. QUBO MODEL AND THE COMPLETE ENCODING SCHEME

The QUBO model is an NP-hard combinatorial problem that consists of minimizing a cost function of the form $C_x = \vec{x}^T \mathcal{A} \vec{x}$, where $\vec{x} \in \{0, 1\}^{n_c}$ is a vector of n_c classical binary variables and \mathcal{A} is a real and symmetric matrix. This model is of particular interest due to its relationship with other optimization problems such as the Max-Cut, portfolio optimization and facility allocation problems [32–34]. Existing metaheuristic approaches such as the TABU search, genetic algorithms, and simulated annealing are capable of finding suitable solutions to problems consisting of $n_c \sim 10^4$ classical variables [35, 36].

In recent implementations of VQA applied to solving QUBO problems, each binary variable in \vec{x} is represented by a single qubit, i.e. $n_q = n_c$; a mapping which we will

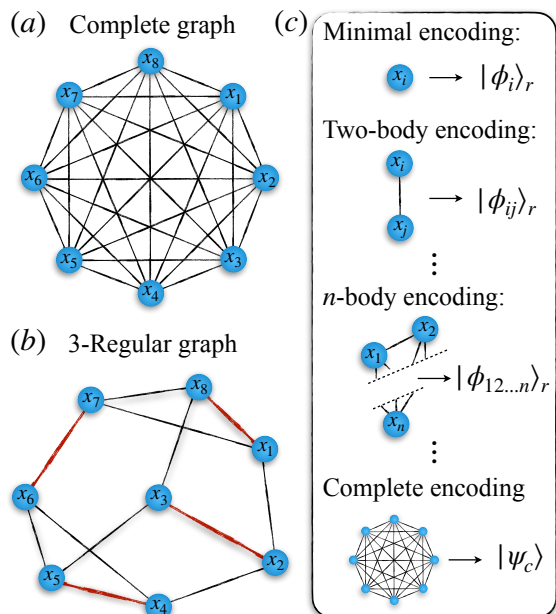


FIG. 1: Schematic representation of the encoding schemes. (a) Complete graph representing a dense QUBO matrix \mathcal{A} . (b) A 3-Regular graph Max-Cut problem. The set of red edges is an example of perfect matching where each vertex is connected to only a single edge. (c) Encoding schemes where n_a -body correlation are encoded with n_a increasing from top to bottom. In the minimal encoding, each of the 2^{n_r} basis states $|\phi_i\rangle$ is used to represent a single classical variable x_i (vertex). In the n -body (two-body) encoding scheme, groups of n (two) classical variables are formed and each basis state represents a unique encoded group. In the complete encoding, each basis state represents an entire graph.

refer to as the *complete encoding*. The resulting quantum state is parameterized by a set of angles $\vec{\theta}$ with the general form

$$|\psi_{\text{cp}}(\vec{\theta})\rangle = \hat{U}_{\text{cp}}(\vec{\theta})|\psi_0\rangle = \sum_{\vec{x} \in \{0,1\}^{n_c}} \alpha_{\vec{x}}(\vec{\theta})|\vec{x}\rangle, \quad (1)$$

where $\hat{U}_{\text{cp}}(\vec{\theta})$ is the unitary evolution implemented on the quantum platform, $\{|\vec{x}\rangle = \otimes_i^{n_q} |x_i\rangle\}$ with $x_i \in \{0, 1\}$ is the complete computational basis spanned by the n_q qubits and $|\psi_0\rangle$ is a given input state. By associating a classical solution \vec{x} with a basis state $|\vec{x}\rangle$, the state $|\psi_{\text{cp}}(\vec{\theta})\rangle$ is able to encode all possible classical solutions in a linear superposition. This unique property of quantum mechanics opens the possibility for multiple classical solutions to be tested simultaneously and this intrinsic parallelism is a strong motivator in developing quantum algorithms for classical problems.

In the case where $\hat{U}_{\text{cp}}(\vec{\theta})$ is a universal quantum circuit, all $\alpha_{\vec{x}}$ in Eq. (1) can in principle be independent (up to the normalization condition). Consequently, this quantum state is able to capture all possible correlations between the classical variables and exhibits expressive power that is beyond classical computation [37–39]. The

goal from here would be to efficiently navigate the exponentially large Hilbert space and reach the basis state(s) which represent the exact or approximate solution(s) to the QUBO problem.

In this complete encoding scheme, the QUBO model can be mapped onto an Ising Hamiltonian

$$\hat{H}_{\text{Ising}} = \frac{1}{4} \sum_{i,j}^{n_c} \mathcal{A}_{ij} (1 - \hat{\sigma}_z^{(i)})(1 - \hat{\sigma}_z^{(j)}), \quad (2)$$

where $\hat{\sigma}_z^{(i)}$ is the z Pauli matrix acting on qubit i and \mathcal{A}_{ij} are the elements of the matrix \mathcal{A} . The ground state of \hat{H}_{Ising} is a basis state $|\vec{x}\rangle$ that corresponds to an exact solution \vec{x} of the QUBO problem defined by \mathcal{A} . For general instances, \hat{H}_{Ising} represents a system of interacting spins where all two-body interactions may be present.

A variational algorithm can then be implemented to find a suitable solution by using the ansatz $\hat{U}_{\text{cp}}(\vec{\theta})$ to produce trial states and finding the set of parameters $\vec{\theta}$ to minimize the cost function

$$C_{\text{cp}}(\vec{\theta}) = \langle \psi_{\text{cp}}(\vec{\theta}) | \hat{H}_{\text{Ising}} | \psi_{\text{cp}}(\vec{\theta}) \rangle. \quad (3)$$

Here, Eq. (3) is a linear function of expectation values with a number of terms polynomial in the number of qubits.

Existing variational ansatzes for optimization problems can be divided in two distinct groups — approaches which require the Hamiltonian \hat{H}_{Ising} to be implemented on the quantum hardware and those which utilize only native gates unconstrained by the specific problem. Approaches such as the QAOA, as implemented in Refs. [20–26], fall into the first category and benefit from being able to exploit some extent of adiabatic computing to search the Hilbert space [40]. In principle, the produced variational state is guaranteed to converge towards the exact solution for infinitely long quantum evolution $\hat{U}_{\text{cp}}(\vec{\theta})$. These approaches however, can be difficult to implement for generic QUBO problems. Approaches that fall into the second category have been implemented in Refs. [27, 28] and are designed to circumvent the technical challenges of implementing \hat{H}_{Ising} . However, these approaches do not guarantee the existence of an efficient path to the optimal solution and can become exponentially hard to optimize as the system size increases.

III. MINIMAL ENCODING

While complete encoding schemes allow for all many-body correlations to be captured between classical variables, the number of qubits required limits their application to small system sizes with unfavorable scaling up perspectives. In what follows, we propose an encoding scheme which sacrifices this ability to capture correlations but allows for problem sizes to be scaled exponentially with the number of qubits. We refer to this mapping as the *minimal encoding*.

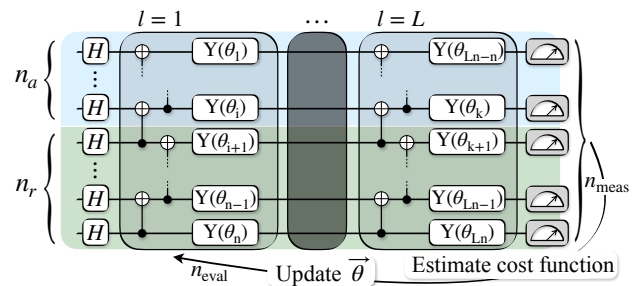


FIG. 2: Hardware-efficient variational ansatz. The initial quantum state $|\psi_0\rangle = \frac{1}{\sqrt{2^{n_q}}} \otimes_{i=1}^{n_q} (|0\rangle + |1\rangle)$ is produced by the first layer of Hadamard gates. Each subsequent layer $1 \leq l \leq L$ is composed of a series of CNOT gates and single rotations $R_y(\theta_i)$ (denoted Y) where the $L \times n_q$ variational parameters are grouped in $\vec{\theta}$ ($n = n_q$ for readability). A single evaluation of the cost function requires n_{meas} measurements in the computational basis and one optimization process requires n_{eval} of these evaluations.

A. Expressibility of the minimal encoding

The minimal encoding scheme considered here requires one ancilla $n_a = 1$ and $n_r = \log_2 n_c$ register qubits for a total number of $n_q = \log_2 n_c + 1$ qubits. The parametrized quantum state can be expressed as

$$|\psi_1(\vec{\theta})\rangle = \sum_{i=1}^{n_c} \beta_i(\vec{\theta}) [a_i(\vec{\theta})|0\rangle_a + b_i(\vec{\theta})|1\rangle_a] \otimes |\phi_i\rangle_r, \quad (4)$$

where the states $\{|\phi_i\rangle_r\}$ ($\{|0\rangle_a, |1\rangle_a\}$) are computational basis states of the register (ancilla) qubits. The premise is to define a one-to-one correspondence between each of the n_c classical variables x_i in \vec{x} and a unique basis state $|\phi_i\rangle_r$, as depicted in Fig. 1 (c). The probability of the i^{th} classical variable to have the value 1 or 0 is given by $\Pr(x_i = 1) = |b_i|^2$ and $\Pr(x_i = 0) = 1 - |b_i|^2 = |a_i|^2$ respectively. The coefficients $\beta_i(\vec{\theta})$ capture the likelihood of measuring each register state $|\phi_i\rangle$ and thus the corresponding state of the ancilla qubit. As an example, encoding the probability distribution over all solutions \vec{x} of dimensions $n_c = 4$ requires $n_r = 2$. One can then define the mapping as $|\phi_1\rangle_r \equiv |00\rangle_r$, $|\phi_2\rangle_r = |01\rangle_r$, $|\phi_3\rangle_r \equiv |10\rangle_r$ and $|\phi_4\rangle_r = |11\rangle_r$. In doing so, the quantum state representing the unit probability of sampling $\vec{x} = (1, 0, 0, 1)$ would read $|\psi_1\rangle = (|1\rangle_a|00\rangle_r + |0\rangle_a|01\rangle_r + |0\rangle_a|10\rangle_r + |1\rangle_a|11\rangle_r)/2$.

The limitation of this compact mapping is its ability to only encode distribution functions of statistically independent classical variables, i.e. where the probability of obtaining a particular classical solution \vec{x} from the state is given by $\Pr(\vec{x}) = \prod_{i=1}^{n_c} \Pr(x_i)$. This comes as no surprise as the quantum state uses only n_c coefficients to encode a probability distribution over 2^{n_c} solutions [46].

B. Cost function to minimize

As with standard VQAs, we defined a cost function to be minimized using a set of parameters $\vec{\theta}$. Given that $|\psi_1(\vec{\theta})\rangle$ represents a distribution function over statistically independent classical variables, it adopts the form

$$C_1(\vec{\theta}) = \sum_{i,j=1}^{n_c} \mathcal{A}_{ij} \frac{\langle \hat{P}_i^1 \rangle_{\vec{\theta}} \langle \hat{P}_j^1 \rangle_{\vec{\theta}}}{\langle \hat{P}_i \rangle_{\vec{\theta}} \langle \hat{P}_j \rangle_{\vec{\theta}}} (1 - \delta_{ij}) + \sum_{i=1}^{n_c} \mathcal{A}_{ii} \frac{\langle \hat{P}_i^1 \rangle_{\vec{\theta}}}{\langle \hat{P}_i \rangle_{\vec{\theta}}}, \quad (5)$$

where $\hat{P}_i = |\phi_i\rangle\langle\phi_i|_r$ ($\hat{P}_i^1 = |1\rangle\langle 1|_a \otimes \hat{P}_i$) are the projectors over the register basis state $|\phi_i\rangle_r$ independent of the ancilla state (with the ancilla being in $|1\rangle_a$). The expectation value can be expressed as $\langle \hat{P}_i \rangle_{\vec{\theta}} = \langle \psi_1(\vec{\theta}) | \hat{P}_i | \psi_1(\vec{\theta}) \rangle$, giving $b_i(\vec{\theta}) = \langle \hat{P}_i^1 \rangle_{\vec{\theta}} / \langle \hat{P}_i \rangle_{\vec{\theta}}$.

The highly entangled quantum state that minimizes Eq. (5) adopts the form $|\psi\rangle = \sum_i \beta_i |\sigma_i\rangle_a \otimes |\phi_i\rangle$ with $\sigma_i = \{0, 1\}$ and corresponds unambiguously to the exact solution $\vec{x} = [\sigma_1, \dots, \sigma_{n_c}]$ that minimizes the QUBO problem defined by the matrix \mathcal{A} . Another important aspect of $C_1(\vec{\theta})$ is that it only depends on the set of norms $\{|b_i|^2\}$. As a consequence, partial tomography performed by a series of measurements solely in the computational basis is sufficient for its estimation. Finally, the cost function $C_1(\vec{\theta})$ in Eq. (5) cannot be reduced to a linear function of expectation values and therefore the QUBO model in the minimal encoding scheme cannot be described with a suitable Hamiltonian. A detailed derivation of Eq. (5) is presented in appendix A.

C. Variational protocol to solve randomly generated QUBO models

The quantum state $|\psi_1(\vec{\theta})\rangle = \hat{U}_1(\vec{\theta})|\psi_0\rangle$ is produced by a parameterized unitary evolution $\hat{U}_1(\vec{\theta})$ applied to a initial product state $|\psi_0\rangle \sim (|0\rangle_a + |1\rangle_a) \otimes \sum_{i=1}^{n_c} |\phi_i\rangle_r$. We consider a hardware efficient circuit as our ansatz $\hat{U}_1(\vec{\theta})$ in the form depicted in Fig. 2. This circuit starts with a layer of Hadamard gates applied to all the qubits initially in $|00\dots 00\rangle$ to produce $|\psi_0\rangle$. It then follows with an alternating sequence of nearest-neighbor CNOT gates and single qubit $R_y(\theta_i)$ rotations. Each successive application of CNOT gates and $R_y(\theta_i)$ rotations make up a single layer. This choice of ansatz represents the simplest case where qubits are arranged in a linear topology with nearest-neighbor couplings. It also produces states with only real-valued coefficients which efficiently restricts the Hilbert space since the cost function in Eq. (5) does not depend on any phases.

The optimization procedure is standard and first consists of randomly choosing a starting point for the variational parameters $\vec{\theta}_{\text{ini}}$ from a uniform distribution and measuring the output quantum state $|\psi(\vec{\theta}_{\text{ini}})\rangle$ in the computational basis. This quantum evolution is repeated

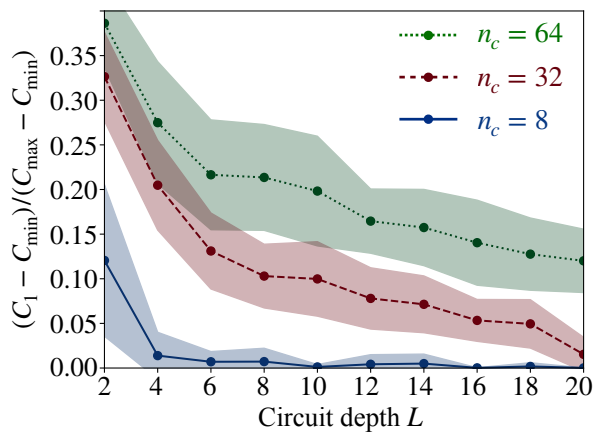


FIG. 3: Optimized cost function value in the minimal encoding scheme as a function of circuit depth L for randomly generated problems of different sizes n_c with $n_{\text{meas}} \rightarrow \infty$. The lines represent the mean final value of 20 runs from 20 different starting points $\vec{\theta}_{\text{ini}}$. The shaded regions show one standard deviation from the mean. The optimization processes have been terminated at $n_{\text{eval}} = 5000$. The minimum and maximum values of the cost function, C_{min} and C_{max} respectively, were found using the classical optimization software Gurobi [41] and were used to normalize the cost function values from 0 to 1.

n_{meas} times to estimate $C_1(\vec{\theta}_{\text{ini}})$. The results are fed to a classical optimizer which updates the parameters $\theta_{\text{old}} \rightarrow \theta_{\text{new}}$. The parameters are updated n_{eval} times until convergence or if a set of termination criteria is met. The resulting parameters are denoted $\vec{\theta}_{\text{opt}}$. From the final quantum state $|\psi(\vec{\theta}_{\text{opt}})\rangle$, a set of solutions $\{\vec{x}\}$ with value $C_x = \vec{x}^T \mathcal{A} \vec{x}$ are obtained by sampling each variable independently following $\text{Pr}(x_i = 1) = |b_i|^2$ [cf. Eq. (4)].

In Fig. 3, we show the average optimized cost function as a function of circuit depth for 3 QUBO instances of different sizes, $n_c = 8, 32$ and 64 , using $n_q = 4, 6$ and 7 qubits respectively. In each instance, the elements of \mathcal{A} were randomly drawn from a uniform distribution ranging from -1 to 1 . COBYLA was chosen as the classical minimizer to update the variational parameters as it was found to give the best results for the least number of cost function evaluations [42].

In Fig. 4 (a)–(c), we compare the infinite-measurement limit to simulated values obtained using $n_{\text{meas}} \sim 1 - 15 \times 10^3$, at specific circuit depths for each of the different problem sizes. Our findings show that increasing the number of measurements reduces the likelihood of the optimizer terminating in a local minima caused by fluctuations in the cost function. It also allows for finer tuning of the optimal parameters due to the increased precision when estimating $C_1(\vec{\theta})$, resulting in an increase in n_{eval} .

The solutions drawn from the optimized states of Fig. 4 (a)–(c) are distributed according to their cost function value in Fig. 4 (d)–(f). The results show that the minimal encoding scheme was able to produce a significant

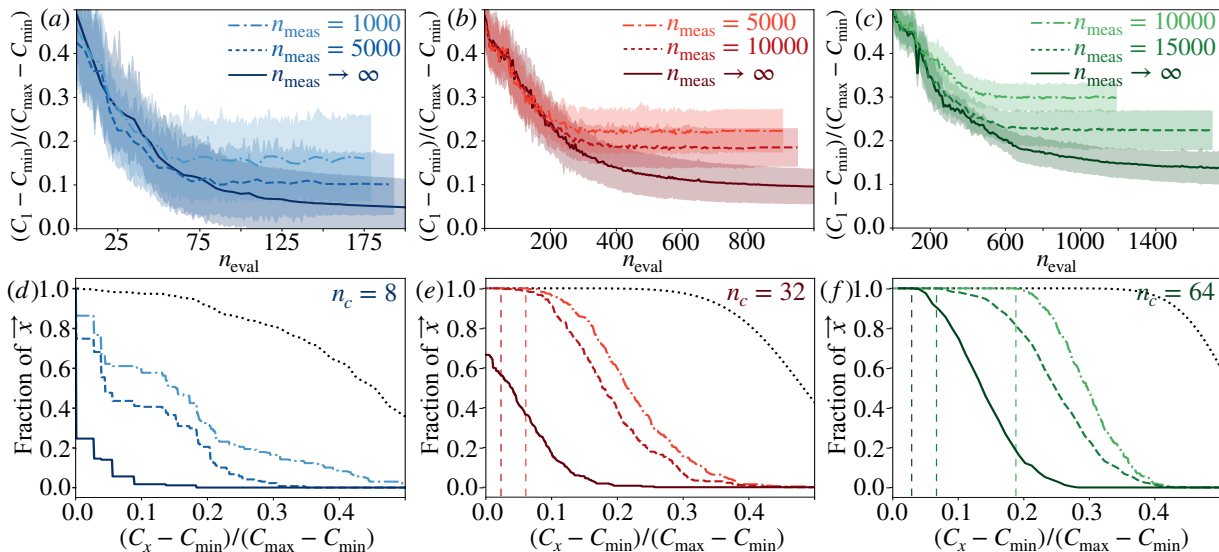


FIG. 4: (a)–(c): Evolution of the (renormalized) cost function $\tilde{C}_1 = (C_1 - C_{\min}) / (C_{\max} - C_{\min})$ during the optimization process in the minimal encoding scheme for different sizes of \mathcal{A} . Shaded regions represent one standard deviation from the average over 30 different starting $\vec{\theta}_{\text{ini}}$. The final value of the cost function decreases as more n_{meas} were used in evaluating \tilde{C}_1 . (a) Circuit depth of $L = 4$ and matrix size of $n_c = 8$ (b) Circuit depth of $L = 12$ and matrix size of $n_c = 32$ (c) Circuit depth of $L = 18$ and matrix size of $n_c = 64$. (d)–(f): Cumulative distribution of solutions drawn from the final quantum state $|\psi_1(\vec{\theta}_{\text{opt}})\rangle$ using the parameters outlined in (a)–(c). The y-axis represents the fraction of solutions with value above the corresponding \tilde{C}_x (x-axis). Vertical lines show the minimum \tilde{C}_1 found from the solutions. The black dotted line shows the distribution of (d) all $2^{n_c} = 256$ solutions and (e)–(f) 4×10^8 randomly generated solutions.

portion of its solutions to be within 20% of the optimal cost function value for $n_c = 8, 32$ and a majority of solutions produced for the $n_c = 64$ case were found to be within 30% of the optimal cost function value. The numerical results also suggest that an increase in resources such as n_{meas} , n_{eval} and depth L are required to maintain comparable accuracy as the problem sizes increase.

IV. TWO-BODY CORRELATIONS

In this section, we show how two-body correlations between the classical variables of the QUBO problem can be introduced into the probability distribution captured by the quantum state. These correlations refer to the conditional probability of one of the variables taking on a certain value given the value of another variable when sampling the classical solution from the probability distribution. We then describe how the particular topology of the different QUBO instances can influence the subset of correlated pairs to be encoded. Specifically, when applied to a Max-Cut problem, we find that encoding only the correlations between pairs of variables that are connected within the graph leads to an improvement in the classical solutions obtained when compared to the minimal encoding approach.

A. General encoding scheme

We propose a general form of the quantum state that allows for the encoding of two-body correlations:

$$|\psi_2(\vec{\theta})\rangle = \sum_{i,j}^{n_{\text{pair}}} \beta_{ij}(\vec{\theta}) [a_{ij}(\vec{\theta}) |00\rangle_a + b_{ij}(\vec{\theta}) |10\rangle_a + c_{ij}(\vec{\theta}) |01\rangle_a + d_{ij}(\vec{\theta}) |11\rangle_a] \otimes |\phi_{ij}\rangle_r, \quad (6)$$

where the register (ancilla) subspace now comprises $n_r = \log_2(n_{\text{pair}})$ ($n_a = 2$) qubits with n_{pair} being the number of two-body correlations encoded. Similar to the minimal encoding scheme, each basis state $|\phi_{ij}\rangle_r$ of the register space acts as a pointer. However, this pointer now points to the index of a pair of classical variables (x_i, x_j) , as depicted in Fig. 1(c). The associated two-qubit ancilla state encodes the bare probability for all pair values, e.g. $\Pr(x_i = 0, x_j = 0) = |a_{ij}|^2$, $\Pr(x_i = 1, x_j = 0) = |b_{ij}|^2$ and so on. This encoding allows one to produce probability distributions that is able to capture correlations beyond statistically independent variables.

The form of Eq. (6) is general enough to allow correlations to be captured between either all pairs of variables or only a subset of these pairs. In certain cases, one might be able to infer a preferred subset of pairs to encode based on the specific topology of the problem, allowing for an important reduction in the number of qubits required. In what follows, we highlight this point by comparing two general cases of frequently encountered QUBO models.

1. Selective subsets for sparse matrices

In QUBO instances where \mathcal{A} is sparse, one might naturally expect that the most important correlations are those between the pairs of non-zero elements in \mathcal{A} . One seminal instance of sparse QUBO models is the d -regular Max-Cut problem where $d \ll n_c$. Each vertex on the corresponding graph is represented by a classical variable in \vec{x} as depicted in Fig. 1 (b), and each edge by a non-zero off-diagonal element in \mathcal{A} . The resulting matrix \mathcal{A} has d unit entries per row and column, and diagonal elements $\mathcal{A}_{i,i} = -d$. By selectively encoding only the $n_{\text{pair}} = n_c \times d/2$ pairs between non-zero elements in \mathcal{A} (i.e. the edges), $n_q = \log_2(n_c \times d) + 1$ are required, which is only $\log_2(d)$ qubits more than the minimal encoding scheme.

Illustrating with an example, encoding the 12 edges of the 3-regular graph with $n_c = 8$ shown in Fig. 1 (b) would require $n_r = 4$ register qubits. The pair (x_1, x_2) could be mapped onto the basis state $|\phi_{12}\rangle_r \equiv |0000\rangle_r$, the pair (x_1, x_7) on $|\phi_{17}\rangle_r \equiv |0001\rangle_r$ and so on until each edge is associated with a unique basis state. In the later sections, we apply this selective encoding method to solve a 3-regular Max-Cut problem with $n_c = 42$ number of variables using $n_q = 8$ qubits, allowing us to surpass the performance of the minimal encoding scheme.

2. Encoding all possible pairings for dense matrices

For more extreme instances where \mathcal{A} is dense, such as the randomly generated QUBO models used in the previous section, selecting a specific subset of two-body correlations becomes completely arbitrary. The only unbiased approach then involves encoding all possible $n_{\text{pair}} = n_c(n_c - 1)/2$ pairs of classical variables, requiring the maximal number of qubits $n_q = \log_2[n_c(n_c - 1)] + 1$. Using this method to encode the 28 edges in the fully connected graph shown Fig. 1 (a) would require $n_r = 5$ register qubits. The mapping would proceed in a similar fashion as before, where the pair (x_1, x_2) can be associated to $|\psi_{12}\rangle_r \equiv |00000\rangle_r$, (x_1, x_3) to $|\psi_{13}\rangle_r \equiv |00001\rangle_r$ and so on. Despite the ‘‘unbiased’’ choice of pairing the variables, capturing all possible two-body correlations for general dense QUBO problems is typically not an efficient use of quantum resource as we shall observe later.

B. Averaging the probabilities and defining the cost function

Interpreting the quantum state $|\psi_2\rangle$ in Eq. (6) as a distribution function $\text{Pr}(\vec{x})$ over the ensemble of classical solutions \vec{x} is not as straightforward as the minimal encoding case. To better understand this statement, let us first consider the limit where the ensemble of pairs $\{(i, j)\}$ encoded would correspond to the set of edges in a 1-regular graph, also known as a perfect matching in

graph theory and highlighted in Fig. 1 (b). In this case, each variable x_i is paired with a single other variable x_j and the probability to sample a solution \vec{x} is uniquely defined as $\text{Pr}(\vec{x}) = \prod_{(i,j)} \text{Pr}(x_i, x_j)$. However, in the more general scenarios where at least one variable is included in more than one pair, the probability of sampling a solution \vec{x} is not uniquely defined anymore. For example, in the limit where all pairs are encoded, there are $N_{\text{pm}}(n_c) = (n_c - 1)!!$ ways of calculating $\text{Pr}(\vec{x})$ with the possibility of vastly different results, where $N_{\text{pm}}(n_c)$ is the number of perfect matchings in a fully connected graph.

In order to be able to define a cost function in the form of Eq. (5) that is well-behaved despite the non-uniqueness of $\text{Pr}(\vec{x})$, we need to define averaged probabilities $\bar{P}_{\sigma_i, \sigma_j}^{i,j}$ of sampling $x_i = \sigma_i$ and $x_j = \sigma_j$ where $\sigma = \{0, 1\}$ that takes into account the multiple ways of calculating $\text{Pr}(\vec{x})$. Doing so, we obtain the averaged probability of sampling $(x_i, x_j) = (1, 1)$ from

$$\bar{P}_{1,1}^{i,j} = \sum_{l \neq i,j} \sum_{k \neq i,j,l}^{n_c} R_{ijkl}(\mathcal{G})(|c_{ki}|^2 + |d_{ki}|^2)(|c_{lj}|^2 + |d_{lj}|^2) + R_{ij}(\mathcal{G})|d_{ij}|^2, \quad (7)$$

where c_{ij} and d_{ij} are the amplitudes of the ancilla states given in Eq. (6) ($\vec{\theta}$ is kept implicit). Here, $R_{ij}(\mathcal{G}) = N_{\text{pm}}(\mathcal{G} - v_i - v_j)/N_{\text{pm}}(\mathcal{G})$ is the ratio between the number of perfect matchings after subtracting the vertices v_i and v_j from the graph \mathcal{G} to the total number of perfect matchings in \mathcal{G} . Similarly, R_{ijkl} describes the same ratio but with 4 vertices removed instead. The graph \mathcal{G} is built by mapping each classical variable to a vertex and each pair encoded in $|\psi_2\rangle$ to an edge. Expressions similar to Eq. (7) for $\bar{P}_{0,0}^{i,j}$, $\bar{P}_{0,1}^{i,j}$ and $\bar{P}_{1,0}^{i,j}$ are derived in appendix A. Using the same approach, one can also derive the averaged probability of sampling $x_i = 1$, leading to

$$\bar{P}_1^i = \sum_{k \neq i}^{n_c} R_{ik}(\mathcal{G})(|b_{ik}|^2 + |d_{ik}|^2), \quad (8)$$

where b_{ij} is also defined in Eq. (6).

In the limit where all possible pairs are encoded, these ratios are $R_{ij}(\mathcal{G}) = (n_c - 3)!/(n_c - 1)! = 1/(n_c - 1)$ and $R_{ijkl}(\mathcal{G}) = R_{ij}(\mathcal{G})/(n_c - 3)$. However, in the case where only a subset of pairs are encoded, $R_{ijkl}(\mathcal{G})$ depends on the vertices $\{i, j, k, l\}$ and is NP-hard to evaluate. One thus needs to resort to approximated ratios and our numerical experiments suggest that estimating $R_{ij}(\mathcal{G}) = 1/d$ and $R_{ijkl}(\mathcal{G}) = R_{ij}(\mathcal{G})/(d - 2)$ for a d -regular graph leads to adequate behaviour of the probabilities.

Having the averaged probabilities defined, one can propose a cost function of the form

$$C_2(\vec{\theta}) = \sum_{i,j=1}^{n_c} A_{ij} \bar{P}_{1,1}^{i,j}(\vec{\theta})(1 - \delta_{ij}) + \sum_{i=1}^{n_c} A_{ii} \bar{P}_1^i(\vec{\theta}). \quad (9)$$

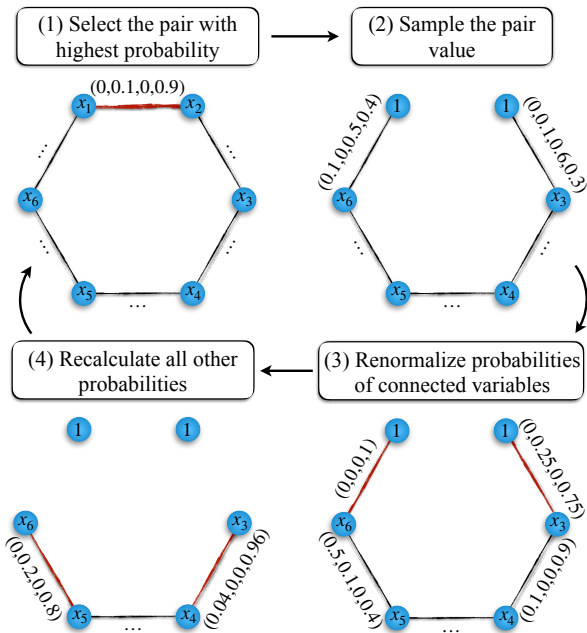


FIG. 5: Schematic of the protocol to sample a solution from the ensemble of two-body correlations. The set of numbers displayed next to the edges between the vertices labeled x_i and x_j represents the probabilities $\bar{P}^{i,j} = (\bar{P}_{0,0}^{i,j}, \bar{P}_{1,0}^{i,j}, \bar{P}_{0,1}^{i,j}, \bar{P}_{1,1}^{i,j})$ with the convention $i < j$. In this example, assuming that $\bar{P}_{1,1}^{1,2} = 0.9$ has the largest probability in the entire graph, (x_1, x_2) would be the first pair to be selected in step (1). The remaining steps are outlined in the main text.

The key properties of Eq. (9) are similar to that of Eq. (5) in that (i) its global minimum corresponds unambiguously to the solution \vec{x} that minimizes the QUBO problem, (ii) it can be estimated by a series of measurements solely in the computational basis, and (iii) it cannot be cast as a linear function of expectation values.

C. Sampling the classical solution from the quantum state

The form of $|\psi_2(\vec{\theta}_{\text{opt}})\rangle$ provides some flexibility in how solutions can be sampled from it. In the following, we describe a sampling protocol that fully exploits the encoded correlations and we show a simple example in Fig. 5.

The procedure is as follows.

1. Select the pair (i, j) with the most definite mean probabilities, i.e. the pair where $\bar{P}_{\sigma_i, \sigma_j}^{i,j}$ of sampling $x_i = \sigma_i$ and $x_j = \sigma_j$ is the closest to unity. As an example, let us consider that the probability to sample $(x_1, x_2) = (1, 1)$, $\bar{P}_{1,1}^{1,2} = 0.9$, is the largest of all mean probabilities, we select the pair $(1, 2)$.
2. Sample the value of the variables from the set of probabilities $\bar{P}^{i,j} = (\bar{P}_{0,0}^{i,j}, \bar{P}_{1,0}^{i,j}, \bar{P}_{0,1}^{i,j}, \bar{P}_{1,1}^{i,j})$.

3. Renormalize the probabilities of all variables connected to the pair evaluated in (2). Following the example, assume that $x_2 = 1$ has been sampled and is connected to the variable x_3 , with probabilities $\bar{P}^{2,3} = (0, 0.1, 0.6, 0.3)$. The probability of sampling $(x_2, x_3) = (0, 1)$, $\bar{P}_{0,1}^{2,3} = 0.6$, is now irrelevant given that $x_2 = 1$, leading to an updated probability of sampling $x_3 = 0$ of 0.25 and $\Pr(x_3 = 1) = 0.75$.
4. Adjust all remaining probabilities $\bar{P}^{k,l}$ consequently. Going back to the example, x_3 is now connected to x_4 where the probabilities were initially $\bar{P}^{3,4} = (0.1, 0, 0, 0.9)$. Since the probability to sample $x_3 = \{0, 1\}$ have been modified as exemplified in (3), $\bar{P}^{3,4}$ is re-evaluated to $(0.04, 0, 0, 0.96)$.
5. Repeat the steps from (1) until all variables have been assigned a value.

Conceptually, this method allows for a finite propagation of correlations along the graph \mathcal{G} during the sampling. As an example, let us consider the case where correlations in the pairs (x_i, x_k) and (x_k, x_l) are explicitly encoded in $|\psi_2\rangle$ but not for the pair of variables (x_i, x_l) . Using this sampling technique makes the probability of sampling $x_l = \{0, 1\}$ change conditionally for the sampled value of x_i , therefore inducing correlations. We stress that these induced correlations are not captured in the optimization process, but only during sampling.

D. Application to randomly generated QUBO instances versus a d-regular Max-Cut

In this section, we present the results obtained after optimizing quantum states of the form of Eq. (6) using the cost function $C_2(\vec{\theta})$ for two different instances of the QUBO model — a 3-regular Max-Cut problem of $n_c = 42$ and a randomly generated matrix \mathcal{A} of $n_c = 8$.

1. Selective encoding for a 3-regular Max-Cut problem

To demonstrate the effectiveness of capturing correlations, we apply our encoding scheme for $n_a = 2$ to a randomly generated 3-regular Max-Cut problem with $n_c = 42$ vertices and 63 edges. In this example, selective encoding was used to only encode correlations between classical variables that are connected by an edge, requiring $n_q = \log_2(63) + 2 \lesssim 8$ qubits. By contrast, encoding all of the 861 possible pairs would require 12 qubits.

Using the same hardware-efficient circuit shown in Fig. 2, we apply the optimization protocol described in Sec. III C. In Fig. 6 (a), we show the final cost function $C_2(\vec{\theta}_{\text{opt}})$ as a function of the circuit depth L in the limit of $n_{\text{meas}} \rightarrow \infty$. We compare to optimization results for the same problem using the minimal encoding scheme

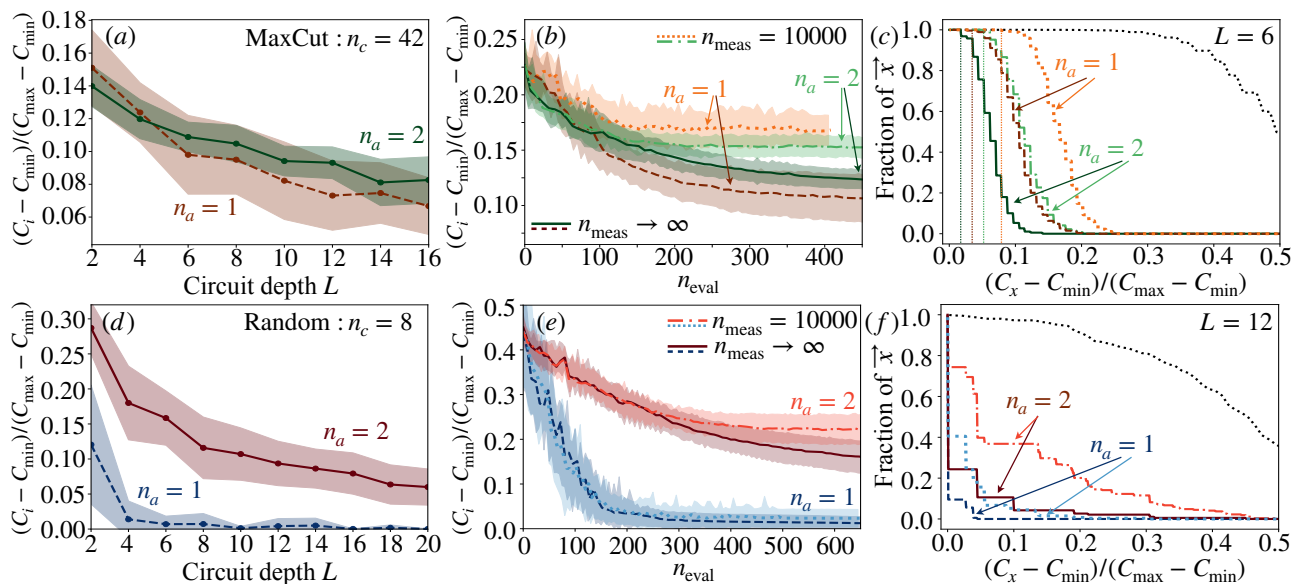


FIG. 6: Comparison of results between $n_a = 1$ and $n_a = 2$ encoding schemes for a randomly generated matrix \mathcal{A} of $n_c = 8$ classical variables with all 28 possible pairings being encoded (top row) and a randomly generated 3-regular Max-Cut problem of $n_c = 42$ using selective encoding to encode only vertices joined by an edge (bottom row). The lighter and darker shaded lines show $n_{\text{meas}} = 15000$ and $n_{\text{meas}} \rightarrow \infty$ respectively. (a),(d) Comparison of final cost function values $C_1(\vec{\theta}_{\text{opt}})$ and $C_2(\vec{\theta}_{\text{opt}})$ as a function of the circuit depth L . Points show the mean value over 30 starting points $\vec{\theta}_{\text{ini}}$. Shaded regions represent one standard deviation from the mean. (b), (e) Comparison of $C_1(\vec{\theta}_{\text{opt}})$ and $C_2(\vec{\theta}_{\text{opt}})$ during the course of optimization. Mean number of evaluations for $n_{\text{meas}} \rightarrow \infty$ extend beyond what is shown. (c),(f) Cumulative distribution of solutions drawn from the optimized quantum states $|\psi_1(\vec{\theta}_{\text{opt}})\rangle$ of (b) and (e) respectively, sorted according to their energy. The black dotted line shows the distribution of (c) all $2^{n_c} = 256$ solutions and (f) 4×10^8 randomly generated solutions.

$n_a = 1$. Panel (b) shows the differences in the optimization process between the $n_a = 1$ and $n_a = 2$ encoding schemes for $L = 6$ for $n_{\text{meas}} \rightarrow \infty$ and $n_{\text{meas}} = 10^4$. While C_1 and C_2 are both depicted in the same figure to demonstrate their respective performance, we stress that they are different quantities and might lead to substantial differences in the quality of the solutions sampled despite their comparable values. This discrepancy is further accentuated given the fundamentally different sampling protocols.

The distribution of solutions drawn from $|\psi_2\rangle$ show a substantial improvement in quality over the solutions obtained from $|\psi_1\rangle$, as depicted in Fig. 6 (c). The use of selective encoding has allowed us to produce better quality solutions through a combination of encoding only the subset of two-body correlations that are expected to be the most relevant and reducing the complexity of the cost function $C_2(\vec{\theta}_{\text{opt}})$.

2. Encoding all pairs for randomly generated QUBO instances

We conclude the results by revisiting the matrix \mathcal{A} with $n_c = 8$ consisting of elements drawn from a continuous uniform probability distribution. In this instance, all 28 possible pairings between the 8 classical variables

are encoded, requiring a total of $n_q = \log_2(28) + 2 \lesssim 7$ qubits.

The results are shown in Fig. 6 (d)–(f) and compared to the results previously obtained in the minimal encoding scheme. Most importantly, panel (c) shows that solutions sampled from the statistically independent distribution function encoded in $|\psi_1\rangle$ are of better quality than those sampled from $|\psi_2\rangle$. These results strongly suggest that encoding all pairs is not an efficient use of quantum resources and can lead to a poorer performance during optimization as well as poorer quality solutions obtained from the final state.

V. GENERALIZATION TO MULTI-BODY CORRELATIONS

Now that we have described in detail a framework to make the first step beyond statistically independent classical variables and encode two-body correlations, generalizing the idea to encoding any set of n_a -body correlations is straightforward. Consider a variational quantum state of the form:

$$|\psi_a(\vec{\theta})\rangle = \sum_i \beta_i(\vec{\theta}) |\varphi_i(\vec{\theta})\rangle_a |\Phi_i\rangle_r, \quad (10)$$

where the ancilla state $|\varphi_i(\vec{\theta})\rangle_a$ is composed of n_a qubits and is associated with a register state $|\Phi_i\rangle_r$ that points

to a specified group i of n_a classical variables. In light of the previous section, whether $|\psi_a(\vec{\theta})\rangle$ can be efficiently optimized to solve a QUBO problem strongly depends on the choice of the encoded groups of n_a classical variables.

One of the simplest mapping strategies consists of encoding a selected set of n_c/n_a independent groups of n_a variables, i.e. where no variable is part of more than one group. The number of qubits needed for this,

$$N_{\text{ind}}(n_a) = \log_2(n_c/n_a) + n_a, \quad (11)$$

increases monotonically until the complete encoding threshold where $n_a = n_c$. In this strategy, there is a one-to-one correspondence between each of the n_c/n_a subgroup of n_a classical variables and a unique basis state of the $n_r = \log_2(n_c/n_a)$ register qubits. The quantum state $|\varphi_i(\vec{\theta})\rangle_a$ of the n_a ancilla qubits associated with the i^{th} subgroup encodes a distribution function that can capture all correlations among the variables of this subgroup. The optimization protocol can be interpreted as partitioning the QUBO problem into subgroups and simultaneously solving each of them using the complete encoding. This choice of mapping is one that is arbitrary as there is no fixed structure as to how the variables should be grouped. However, the minimal use of quantum resources might make this a desirable choice in certain situations.

Another strategy would be to encode all $\frac{n_c!}{n_a!(n_c-n_a)!}$ groups of n_a variables, which is the generalization of encoding all possible pairs for $n_a = 2$. This requires

$$N_{\text{all}}(n_a) = \log_2\left(\frac{n_c!}{n_a!(n_c-n_a)!}\right) + n_a \quad (12)$$

qubits, which is a non-monotonic function of n_a and can substantially exceed the total number of qubits required for the complete encoding, showing an inefficient use of quantum resource.

In between these two extremes are multiple mapping options and whether any of these encoding schemes can efficiently exploit the dominant correlations within a specific family of QUBO models is of great interest. For example, one could imagine encoding an ensemble of $(d+1)$ -body correlations that follows the specific topology of a d -regular Max-Cut problem. In this case, each classical variable within the d -regular graph forms a group of $d+1$ elements. Encoding all of those n_c groups into a quantum state would require

$$N_{\text{reg}}(n_a) = \log_2(n_c) + n_a + 1, \quad (13)$$

qubits, where $d = n_a$. For $n_a \rightarrow (n_c - 1)$, i.e. a fully connected graph, the number of qubits exceeds the threshold $n_q = n_c$ by $\log_2(n_c)$.

VI. CONCLUSION

In this work, we have proposed and analysed a systematic encoding scheme for variational quantum algorithms that allows one to capture increasing amount of

correlations between classical variables in optimization problems. We first detailed the implementation of the minimal encoding scheme, using only $n_q = \log_2(n_c) + 1$ qubits to solve a QUBO model of size n_c . Our numerical solutions show that when applied to randomly generated problem instances of size $n_c = 8, 32$ and 64 , this encoding scheme was able to find suitable high quality solutions using resources compatible with NISQ devices despite the inability to capture any correlations between the classical variables.

We also detailed encoding protocols that allow for two-body correlations to be captured between the classical variables. The number of qubits required scales logarithmically with the number of pairs encoded and we showed that exploiting the topology of the QUBO instance is essential for efficient optimization of the quantum state. By applying the two-body correlation encoding to a Max-Cut problem of 42 vertices, we were able to obtain better performance compared to the minimal encoding scheme.

The focus of this work was primarily on the encoding schemes outlined in the main text and was not intended as a thorough investigation of the most efficient optimization protocols. We believe that the results presented can still be improved upon substantially. One possible area for exploration could be finding an ansatz that would result in a smoother cost function landscape with shallower circuits. A more adapted classical optimizer may also bring significant improvements in the optimization process as it was found that a considerable fraction of optimization runs got stuck in local minimas [43, 44].

Further avenues to explore would be whether generalizations to larger n_a -body correlations can be efficiently optimized and whether alternative ways of capturing correlations for dense problem instances can be found. Lastly, and perhaps most importantly, would be to explore whether these encoding protocols can be implemented on quantum platforms of sizes that cannot be classically simulated to provide a quantum advantage over existing classical algorithms.

VII. ACKNOWLEDGMENTS

This research is supported by the National Research Foundation, Prime Ministers Office, Singapore and the Ministry of Education, Singapore under the Research Centres of Excellence programme. It was also partially funded by Polisimulator project co-financed by Greece and the EU Regional Development Fund, the European Research Council under the European Unions Seventh Framework Programme (FP7/2007-2013).

Appendix A: Derivation of the cost functions

In all of the encoding schemes outlined in the main text, the quantum state $|\psi(\vec{\theta})\rangle$ captures a probability distribution over all 2^{n_c} classical solutions. In this context,

we generalize the QUBO cost function, $C_x = \vec{x}^\top A \vec{x}$, as a sum over all possible solutions weighted by their respective probability to be sampled, i.e.

$$\begin{aligned} \mathcal{C} &= \sum_{\{\vec{x}\}} \vec{x}^\top A \vec{x} \Pr(\vec{x}), \\ &= \sum_{\{\vec{x}\}} \sum_{i,j=1}^{n_c} x_i \mathcal{A}_{ij} x_j \Pr(\vec{x}), \\ &= \sum_{i,j=1}^{n_c} \mathcal{A}_{ij} \sum_{\{\vec{x}|x_i=x_j=1\}} \Pr(\vec{x}). \end{aligned} \quad (\text{A1})$$

Here, $\{\vec{x}\}$ represents the ensemble of all the 2^{n_c} possible solutions \vec{x} while $\{\vec{x}|x_i=x_j=1\}$ represents only the subset of the 2^{n_c-2} solutions where the i^{th} and j^{th} variables in \vec{x} are $x_i=x_j=1$. To obtain the third line, we have explicitly used the fact that only variables with values equal to 1 contributes to the cost function. In what follows, we present in more details the following steps that lead to Eqs. (5) and (9) of the main text and provide further discussions about their properties.

1. Minimal encoding

In the minimal encoding, the state $|\psi_1(\vec{\theta})\rangle$ describes statistically independent classical variables where the probability of sampling \vec{x} is $\Pr(\vec{x}) = \prod_{i=1}^{n_c} \Pr(x_i)$. In this case,

$$\sum_{\{\vec{x}|x_i=x_j=1\}} \Pr(\vec{x}) = \begin{cases} \Pr(x_i=1)\Pr(x_j=1) & \text{if } i \neq j \\ \Pr(x_i=1) & \text{if } i = j \end{cases}, \quad (\text{A2})$$

which, in terms of the quantum state amplitudes, reads

$$\sum_{\{\vec{x}|x_i=x_j=1\}} \Pr(\vec{x}) = \begin{cases} |b_i(\vec{\theta})|^2 |b_j(\vec{\theta})|^2 & \text{if } i \neq j \\ |b_i(\vec{\theta})|^2 & \text{if } i = j \end{cases}. \quad (\text{A3})$$

By substituting these results into Eq. (A1), one gets

$$C_1(\vec{\theta}) = \sum_{i,j=1}^{n_c} \mathcal{A}_{ij} |b_i(\vec{\theta})|^2 |b_j(\vec{\theta})|^2 (1 - \delta_{ij}) + \sum_{i=1}^{n_c} \mathcal{A}_{ii} |b_i(\vec{\theta})|^2. \quad (\text{A4})$$

The final form presented in Eq. (5) of the main text is obtained by expressing the probabilities $|b_i(\vec{\theta})|^2 = \langle \hat{P}_i^1 \rangle_{\vec{\theta}} / \langle \hat{P}_i \rangle_{\vec{\theta}}$ in terms of the projectors \hat{P}_i and \hat{P}_i^1 (defined in the main text).

2. Two-body correlations

In the case where the variational quantum state $|\psi_2(\vec{\theta})\rangle$ encodes a given set of two-body correlations, evaluating Eq. (A1) is not as straightforward as in the minimal encoding. This is due to the multiple ways of evaluating the probability $\Pr(\vec{x})$ of sampling a solution \vec{x} , each of which capable of producing very different results. More precisely, for $\vec{x} = (\sigma_1, \sigma_2, \dots, \sigma_{n_c})$, $\Pr(\vec{x}) = \prod_{\{(i,j)\}} \Pr(x_i = \sigma_i | x_j = \sigma_j)$ where $\Pr(x_i = \sigma_i | x_j = \sigma_j)$ represents the conditional probability to sample $x_i = \sigma_i$ given $x_j = \sigma_j$. Here the ensemble $\{(i,j)\}$ represents a set of independent encoded pairs where no variables are repeated, i.e. a perfect matching. Consequently, there are as many ways to evaluate $\Pr(\vec{x})$ as there are perfect matchings $N_{\text{pm}}(\mathcal{G})$ in the graph \mathcal{G} , corresponding to the encoded pairs in $|\psi_2(\vec{\theta})\rangle$.

To evaluate Eq. (A1), we average over all possible ways of evaluating $\Pr(\vec{x})$, denoted by $\{\Pr(\vec{x})\}$, and define the mean probabilities

$$\bar{P}_{1,1}^{i,j} \equiv \frac{1}{N_{\text{pm}}(\mathcal{G})} \sum_{\{\Pr(\vec{x})\}} \sum_{\{\vec{x}|x_i=x_j=1\}} \Pr(\vec{x}), \quad (\text{A5})$$

for $i \neq j$. The mean probability to sample a single variable $x_i = 1$, \bar{P}_1^i , is given by the same above definition with $i = j$. There are two distinct scenarios that one can encounter while averaging over all possible perfect matchings corresponding to $x_i = x_j = 1$ in \mathcal{G} . The first is when the perfect matching contains an edge connecting x_i and x_j . There are $N_{\text{pm}}(\mathcal{G}_{ij})$ of such instances, where \mathcal{G}_{ij} is the graph obtained by subtracting the two vertices i and j . For each of these instances, the conditional probability $\Pr(x_i = 1 | x_j = 1) = |d_{ij}(\vec{\theta})|^2$ is directly encoded in the quantum state (see Eq. (6) of the main text). The second scenario occurs when the perfect matching does not include an edge connecting the vertices i and j to each other but instead to other vertices k and l . These cases appear within a subset of $N_{\text{pm}}(\mathcal{G}_{ijkl})$ perfect matching instances, where \mathcal{G}_{ijkl} is the graph obtained by subtracting the vertices i, j, k and l . In these scenarios, the conditional probability $\Pr(x_i = 1 | x_j = 1)$ is not directly encoded in the quantum state and has to be inferred from $\Pr(x_i = 1 | x_j = 1) = \Pr(x_k = 0, 1 | x_i = 1) \Pr(x_l = 0, 1 | x_j = 1) = (|c_{ki}|^2 + |d_{ki}|^2)$, where $\Pr(x_k = 0, 1 | x_i = 1)$ is the conditional probability of having $x_k = 0$ or $x_k = 1$ given $x_i = 1$.

Considering these contributions, we obtain the following mean conditional probabilities:

$$\begin{aligned}
\bar{P}_{1,1}^{i,j} &= \frac{N_{\text{pm}}(\mathcal{G}_{ijkl})}{N_{\text{pm}}(\mathcal{G})} \sum_{l \neq i,j}^{n_c} \sum_{k \neq i,j,l}^{n_c} \Pr(x_k = 0, 1|x_i = 1) \Pr(x_l = 0, 1|x_j = 1) + \frac{N_{\text{pm}}(\mathcal{G}_{ij})}{N_{\text{pm}}(\mathcal{G})} \Pr(x_i = 1|x_j = 1), \\
&= \frac{N_{\text{pm}}(\mathcal{G}_{ijkl})}{N_{\text{pm}}(\mathcal{G})} \sum_{l \neq i,j}^{n_c} \sum_{k \neq i,j,l}^{n_c} [(|c_{ki}|^2 + |d_{ki}|^2) (|c_{lj}|^2 + |d_{lj}|^2)] + \frac{N_{\text{pm}}(\mathcal{G}_{ij})}{N_{\text{pm}}(\mathcal{G})} |d_{ij}|^2,
\end{aligned} \tag{A6}$$

for $(i \neq j)$, and

$$\begin{aligned}
\bar{P}_{1,1}^i &= \frac{N_{\text{pm}}(\mathcal{G}_{ik})}{N_{\text{pm}}(\mathcal{G})} \sum_{i \neq k}^{n_c} \Pr(x_k = 0, 1|x_i = 1), \\
&= \frac{N_{\text{pm}}(\mathcal{G}_{ik})}{N_{\text{pm}}(\mathcal{G})} \sum_{i \neq k}^{n_c} (|c_{ki}|^2 + |d_{ki}|^2),
\end{aligned} \tag{A7}$$

for $i = j$.

The cost function in Eq. (A1) thus adopts the final form

$$C_2 = \sum_{i,j=1}^{n_c} \mathcal{A}_{ij} \bar{P}_{1,1}^{i,j} (1 - \delta_{ij}) + \sum_{i=1}^{n_c} \mathcal{A}_{ii} \bar{P}_{1,1}^i, \tag{A8}$$

as in Eq. (9) of the main text.

This averaging ensures a well behaved cost function where the quantum state which minimizes this cost function gives the unit probability of sampling the exact solution which minimizes the QUBO problem. The drawback of this method is the partial “washing out” of the encoded correlations as it can be seen by the first term (second scenario) in Eq. (A6) which adopts the form of two statistically independent variables.

Following the steps outlined above, the following averaged probabilities can also be derived:

$$\begin{aligned}
\bar{P}_{0,1}^{i,j} &= \sum_{l \neq i,j}^{n_c} \sum_{k \neq i,j,l}^{n_c} R_{ijkl}(\mathcal{G}) (|a_{ki}|^2 + |b_{ki}|^2) (|c_{lj}|^2 + |d_{lj}|^2) \\
&\quad + R_{ij}(\mathcal{G}) |c_{ij}|^2,
\end{aligned} \tag{A9}$$

$$\begin{aligned}
\bar{P}_{1,0}^{i,j} &= \sum_{l \neq i,j}^{n_c} \sum_{k \neq i,j,l}^{n_c} R_{ijkl}(\mathcal{G}) (|c_{ki}|^2 + |d_{ki}|^2) (|a_{lj}|^2 + |b_{lj}|^2) \\
&\quad + R_{ij}(\mathcal{G}) |b_{ij}|^2,
\end{aligned} \tag{A10}$$

$$\bar{P}_{0,0}^{i,j} = 1 - \left[\bar{P}_{0,1}^{i,j} - \bar{P}_{1,0}^{i,j} - \bar{P}_{1,1}^{i,j} \right]. \tag{A11}$$

3. The cost function landscape

The cost functions $C_1(\vec{\theta})$ and $C_2(\vec{\theta})$, described by Eq. (5) and Eq. (9) of the main text, are nonlinear combinations of expectation values. This form leads to very different behaviours as a function of $\vec{\theta}$ when compared to

the linear cost function $C_{\text{cp}}(\vec{\theta})$ derived in the complete encoding limit [cf. Eq. (3) of the main text].

These differences are depicted in Fig. 7, where $C_{\text{cp}}(\vec{\theta})$, $C_1(\vec{\theta})$ and $C_2(\vec{\theta})$ are plotted as a function of a single parameter θ_i with all other rotation angles being fixed at random values. The \mathcal{A} matrix used in Fig. 7 (a)–(c) is the same randomly generated $n_c = 8$ matrix used in Section III C of the main text, while the same \mathcal{A} matrix describing the $n_c = 42$ 3-regular Max-Cut in Section IV A 1 was used in panel (d). The circuit used to obtain the landscape of $C_{\text{cp}}(\theta_i)$ consists of a single layer of $R_Y(\theta)$ applied in parallel to all qubits. This circuit was chosen as it consists of only single-qubit rotations with no entangling gates. The resulting quantum state can therefore only describe probability distributions of statistically independent classical variables in the complete encoding, and is equally expressible as $|\psi_1(\vec{\theta})\rangle$ in the minimal encoding.

For deep circuits and linear cost functions, Ref. [31] predicts the existence of barren plateaus for 2-design quantum circuits $\hat{U}(\vec{\theta})$. Interestingly, the non linear forms of $C_1(\vec{\theta})$ and $C_2(\vec{\theta})$ do not fulfil the necessary conditions underlying the proof derived in Ref. [31]. Consequently, we expect that a more constrained condition of a t -design quantum circuit, where $t > 2$, would be necessary to demonstrate the existence of these barren plateaus. In addition, for cost functions comprising of a linear combination of a $Poly(n_q)$ number of global observables, Ref. [45] predicts the existence of barren plateaus even for shallow circuits. Despite the fact that each observable considered in this work is a projector, i.e. global operator, the nonlinearity of $C_1(\vec{\theta})$ and $C_2(\vec{\theta})$ combined with the $\mathcal{O}(2^{n_q})$ number of terms involved also do not fulfil the necessary conditions for the proof in Ref. [45]. A more thorough investigation of the barren plateaus for nonlinear cost function is left for future work.

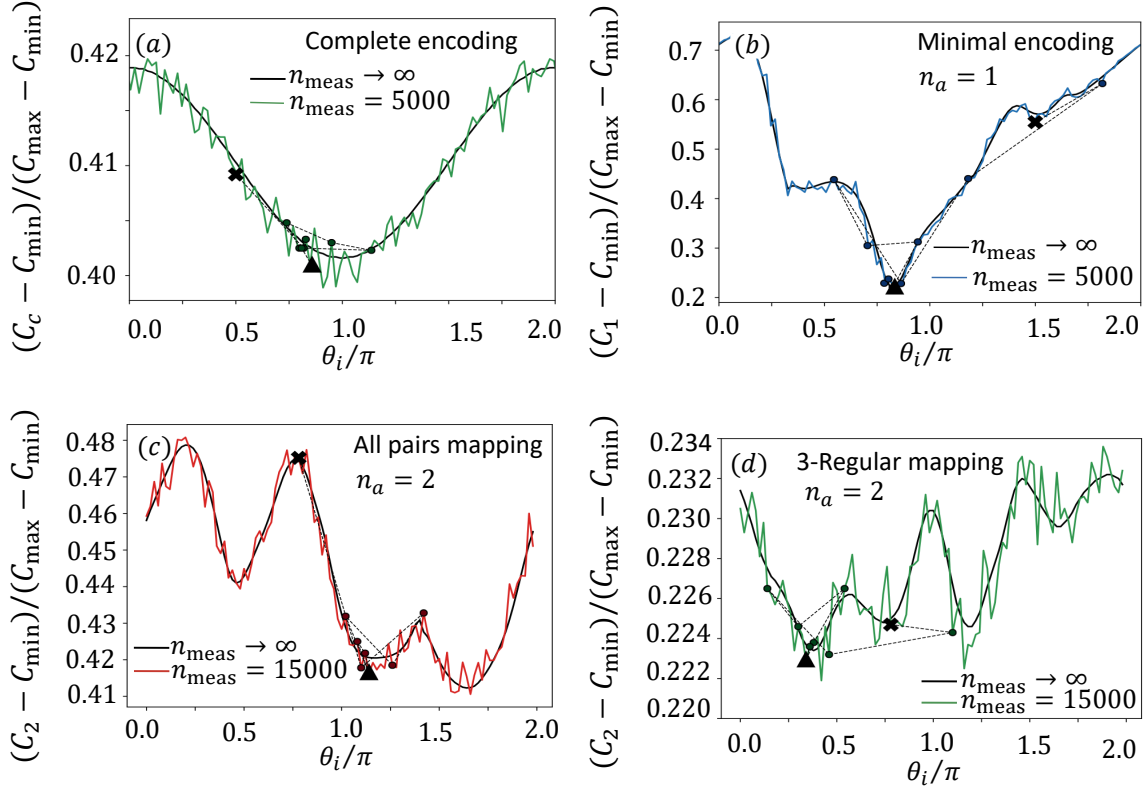


FIG. 7: Cost function landscape as a function of a randomly chosen θ_i . Solid line shows the expectation value in the limit $n_{\text{meas}} \rightarrow \infty$, compared with the simulated value obtained from finite n_{meas} . The dotted lines from the cross to the triangle show the path taken by the COBYLA optimizer to find the optimal θ_i . (a)–(b) Complete and minimal encoding cost functions, $C_{\text{cp}}(\vec{\theta})$ and $C_1(\vec{\theta})$, for a randomly generated \mathcal{A} with $n_c = 8$. Simulated values obtained using $n_{\text{meas}} = 5000$ and circuit depth $L = 4$. $n_q = 8$ qubits were used for the complete encoding compared to $n_q = 4$ in the minimal encoding. (c) $C_2(\vec{\theta})$ for a randomly generated \mathcal{A} with $n_c = 8$ using $n_a = 2$ encoding scheme. All possible two-body correlations were encoded using $n_q = 7$ qubits. Simulated values obtained using $n_{\text{meas}} = 15000$ and circuit depth $L = 12$. (d) $C_2(\vec{\theta})$ for a 3-regular Max-Cut problem with $n_c = 42$ classical variables using $n_a = 2$ encoding scheme. Selective encoding with $n_q = 8$ qubits was used. Simulated values obtained using $n_{\text{meas}} = 15000$ and circuit depth $L = 6$.

-
- [1] M Saffman. Quantum computing with atomic qubits and rydberg interactions: progress and challenges. *Journal of Physics B: Atomic, Molecular and Optical Physics*, 49(20):202001, oct 2016.
- [2] G Wendin. Quantum information processing with superconducting circuits: a review. *Reports on Progress in Physics*, 80(10):106001, sep 2017.
- [3] Colin D. Bruzewicz, John Chiaverini, Robert McConnell, and Jeremy M. Sage. Trapped-ion quantum computing: Progress and challenges. *Applied Physics Reviews*, 6(2):021314, 2019.
- [4] Frank Arute, Kunal Arya, Ryan Babbush, Dave Bacon, Joseph C. Bardin, Rami Barends, Rupak Biswas, Sergio Boixo, Fernando G. S. L. Brandao, David A. Buell, Brian Burkett, Yu Chen, Zijun Chen, Ben Chiaro, Roberto Collins, William Courtney, Andrew Dunsworth, Edward Farhi, Brooks Foxen, Austin Fowler, Craig Gidney, Marissa Giustina, Rob Graff, Keith Guerin, Steve Habegger, Matthew P. Harrigan, Michael J. Hartmann, Alan Ho, Markus Hoffmann, Trent Huang, Travis S. Humble, Sergei V. Isakov, Evan Jeffrey, Zhang Jiang, Dvir Kafri, Kostyantyn Kechedzhi, Julian Kelly, Paul V. Klimov, Sergey Knysh, Alexander Korotkov, Fedor Kostritsa, David Landhuis, Mike Lindmark, Erik Lucero, Dmitry Lyakh, Salvatore Mandrà, Jarrod R. McClean, Matthew McEwen, Anthony Megrant, Xiao Mi, Kristel Michielsen, Masoud Mohseni, Josh Mutus, Ofer Naaman, Matthew Neeley, Charles Neill, Murphy Yuezhen Niu, Eric Ostby, Andre Petukhov, John C. Platt, Chris Quintana, Eleanor G. Rieffel, Pedram Roushan, Nicholas C. Rubin, Daniel Sank, Kevin J. Satzinger, Vadim Smelyanskiy, Kevin J. Sung, Matthew D. Trevithick, Amit Vainsencher, Benjamin Villalonga, Theodore White, Z. Jamie Yao, Ping Yeh, Adam Zalcman, Hartmut Neven, and John M. Martinis. Quantum supremacy using a programmable superconducting processor. *Nature*, 574(7779):505–510, 2019.
- [5] Engineering National Academies of Sciences and

- Medicine. *Quantum Computing: Progress and Prospects*. The National Academies Press, Washington, DC, 2019.
- [6] Jianwei Wang, Fabio Sciarrino, Anthony Laing, and Mark G. Thompson. Integrated photonic quantum technologies. *Nature Photonics*, 14(5):273–284, 2020.
- [7] Peter W. Shor. Polynomial-time algorithms for prime factorization and discrete logarithms on a quantum computer. *SIAM Journal on Computing*, 26(5):1484–1509, 1997.
- [8] Lov K. Grover. Quantum mechanics helps in searching for a needle in a haystack. *Phys. Rev. Lett.*, 79:325–328, Jul 1997.
- [9] John Preskill. Quantum Computing in the NISQ era and beyond. *Quantum*, 2:79, August 2018.
- [10] Bela Bauer, Sergey Bravyi, Mario Motta, and Garnet Kin-Lic Chan. Quantum algorithms for quantum chemistry and quantum materials science. *arXiv preprint arXiv:2001.03685*, 2020.
- [11] Sam McArdle, Suguru Endo, Alán Aspuru-Guzik, Simon C. Benjamin, and Xiao Yuan. Quantum computational chemistry. *Rev. Mod. Phys.*, 92:015003, Mar 2020.
- [12] Edward Farhi, Jeffrey Goldstone, and Sam Gutmann. A quantum approximate optimization algorithm. *arXiv preprint arXiv:1411.4028*, 2014.
- [13] Alberto Peruzzo, Jarrod McClean, Peter Shadbolt, Man-Hong Yung, Xiao-Qi Zhou, Peter J. Love, Alán Aspuru-Guzik, and Jeremy L. O’Brien. A variational eigenvalue solver on a photonic quantum processor. *Nature Communications*, 5(1):4213, 2014.
- [14] Jarrod R McClean, Jonathan Romero, Ryan Babbush, and Alán Aspuru-Guzik. The theory of variational hybrid quantum-classical algorithms. *New Journal of Physics*, 18(2):023023, feb 2016.
- [15] Abhinav Kandala, Antonio Mezzacapo, Kristan Temme, Maika Takita, Markus Brink, Jerry M. Chow, and Jay M. Gambetta. Hardware-efficient variational quantum eigensolver for small molecules and quantum magnets. *Nature*, 549(7671):242–246, 2017.
- [16] Nikolaž Moll, Panagiotis Barkoutsos, Lev S Bishop, Jerry M Chow, Andrew Cross, Daniel J Egger, Stefan Filipp, Andreas Fuhrer, Jay M Gambetta, Marc Ganzhorn, Abhinav Kandala, Antonio Mezzacapo, Peter Mller, Walter Riess, Gian Salis, John Smolin, Ivano Tavernelli, and Kristan Temme. Quantum optimization using variational algorithms on near-term quantum devices. *Quantum Science and Technology*, 3(3):030503, jun 2018.
- [17] Troels F. Rønnow, Zhihui Wang, Joshua Job, Sergio Boixo, Sergei V. Isakov, David Wecker, John M. Martinis, Daniel A. Lidar, and Matthias Troyer. Defining and detecting quantum speedup. *Science*, 345(6195):420–424, 2014.
- [18] Edward Farhi, Jeffrey Goldstone, and Sam Gutmann. A quantum approximate optimization algorithm applied to a bounded occurrence constraint problem. *arXiv preprint arXiv:1412.6062*, 2014.
- [19] Edward Farhi, Jeffrey Goldstone, Sam Gutmann, and Leo Zhou. The quantum approximate optimization algorithm and the sherrington-kirkpatrick model at infinite size. *arXiv preprint arXiv:1910.08187*, 2019.
- [20] J. S. Otterbach, R. Manenti, N. Alidoust, A. Bestwick, M. Block, B. Bloom, S. Caldwell, N. Didier, E. Schuyler Fried, S. Hong, P. Karalekas, C. B. Osborn, A. Pappageorge, E. C. Peterson, G. Prawiroatmodjo, N. Rubin, Colm A. Ryan, D. Scarabelli, M. Scheer, E. A. Sete, P. Sivarajah, Robert S. Smith, A. Staley, N. Tezak, W. J. Zeng, A. Hudson, Blake R. Johnson, M. Reagor, M. P. da Silva, and C. Rigetti. Unsupervised machine learning on a hybrid quantum computer. *arXiv preprint arXiv:1712.05771*, 2017.
- [21] Xiaogang Qiang, Xiaoqi Zhou, Jianwei Wang, Callum M. Wilkes, Thomas Loke, Sean O’Gara, Laurent Kling, Graham D. Marshall, Raffaele Santagati, Timothy C. Ralph, Jingbo B. Wang, Jeremy L. O’Brien, Mark G. Thompson, and Jonathan C. F. Matthews. Large-scale silicon quantum photonics implementing arbitrary two-qubit processing. *Nature Photonics*, 12(9):534–539, 2018.
- [22] G. Pagano, A. Bapat, P. Becker, K. S. Collins, A. De, P. W. Hess, H. B. Kaplan, A. Kyprianidis, W. L. Tan, C. Baldwin, L. T. Brady, A. Deshpande, F. Liu, S. Jordan, A. V. Gorshkov, and C. Monroe. Quantum approximate optimization of the long-range ising model with a trapped-ion quantum simulator. *arXiv preprint arXiv:1906.02700*, 2019.
- [23] Andreas Bengtsson, Pontus Vikstl, Christopher Warren, Marika Svensson, Xiu Gu, Anton Frisk Kockum, Philip Krantz, Christian Krian, Daryoush Shiri, Ida-Maria Svensson, Giovanna Tancredi, Gran Johansson, Per Delsing, Giulia Ferrini, and Jonas Bylander. Quantum approximate optimization of the exact-cover problem on a superconducting quantum processor. *arXiv preprint arXiv:1912.10495*, 2019.
- [24] Deanna M. Abrams, Nicolas Didier, Blake R. Johnson, Marcus P. da Silva, and Colm A. Ryan. Implementation of the xy interaction family with calibration of a single pulse. *arXiv preprint arXiv:1912.04424*, 2019.
- [25] Madita Willsch, Dennis Willsch, Fengping Jin, Hans De Raedt, and Kristel Michielsen. Benchmarking the quantum approximate optimization algorithm. *Quantum Information Processing*, 19:197, 2020.
- [26] Frank Arute, Kunal Arya, Ryan Babbush, Dave Bacon, Joseph C. Bardin, Rami Barends, Sergio Boixo, Michael Broughton, Bob B. Buckley, David A. Buell, Brian Burkett, Nicholas Bushnell, Yu Chen, Zijun Chen, Ben Chiaro, Roberto Collins, William Courtney, Sean Demura, Andrew Dunsworth, Edward Farhi, Austin Fowler, Brooks Foxen, Craig Gidney, Marissa Giustina, Rob Graff, Steve Habegger, Matthew P. Harrigan, Alan Ho, Sabrina Hong, Trent Huang, L. B. Ioffe, Sergei V. Isakov, Evan Jeffrey, Zhang Jiang, Cody Jones, Dvir Kafri, Kostyantyn Kechedzhi, Julian Kelly, Seon Kim, Paul V. Klimov, Alexander N. Korotkov, Fedor Kostritsa, David Landhuis, Pavel Laptev, Mike Lindmark, Martin Leib, Erik Lucero, Orion Martin, John M. Martinis, Jarrod R. McClean, Matt McEwen, Anthony Megrant, Xiao Mi, Masoud Mohseni, Wojciech Mroczkiewicz, Josh Mutus, Ofer Naaman, Matthew Neeley, Charles Neill, Florian Neukart, Hartmut Neven, Murphy Yuezhen Niu, Thomas E. O’Brien, Bryan O’Gorman, Eric Ostby, Andre Petukhov, Harald Putterman, Chris Quintana, Pedram Roushan, Nicholas C. Rubin, Daniel Sank, Kevin J. Satzinger, Andrea Skolik, Vadim Smelyanskiy, Doug Strain, Michael Streif, Kevin J. Sung, Marco Szalay, Amit Vainsencher, Theodore White, Z. Jamie Yao, Ping Yeh, Adam Zalcman, and Leo Zhou. Quantum approximate optimization of non-planar graph problems on a planar superconducting processor. *arXiv preprint arXiv:2004.04197*, 2020.
- [27] Arthur G. Rattew, Shaohan Hu, Marco Pistoia, Richard

- Chen, and Steve Wood. A domain-agnostic, noise-resistant, hardware-efficient evolutionary variational quantum eigensolver. *arXiv preprint arXiv:1910.09694*, 2019.
- [28] Lee Braine, Daniel J Egger, Jennifer Glick, and Stefan Woerner. Quantum algorithms for mixed binary optimization applied to transaction settlement. *arXiv preprint arXiv:1910.05788*, 2019.
- [29] Michael R Garey and David S Johnson. *Computers and intractability*, volume 174. freeman San Francisco, 1979.
- [30] Leo Zhou, Sheng-Tao Wang, Soonwon Choi, Hannes Pichler, and Mikhail D. Lukin. Quantum approximate optimization algorithm: Performance, mechanism, and implementation on near-term devices. *arXiv preprint arXiv:1812.01041*, 2018.
- [31] Jarrod R. McClean, Sergio Boixo, Vadim N. Smelyanskiy, Ryan Babbush, and Hartmut Neven. Barren plateaus in quantum neural network training landscapes. *Nature Communications*, 9(1):4812, 2018.
- [32] Richard M. Karp. *Reducibility among Combinatorial Problems*, pages 85–103. Springer US, Boston, MA, 1972.
- [33] Harry Markowitz. Portfolio selection. *The Journal of Finance*, 7(1):77–91, 1952.
- [34] Tjalling C. Koopmans and Martin Beckmann. Assignment problems and the location of economic activities. *Econometrica*, 25(1):53–76, 1957.
- [35] Dimitris Fouskakis and David Draper. Stochastic optimization: a review. *International Statistical Review*, 70(3):315–349, 2002.
- [36] F. Glover M. Lewis Z.P Lü H.B Wang Y. Wang G. Kochenberger, J.K. Hao. The unconstrained binary quadratic programming problem: a survey. *Journal of Combinatorial Optimization*, 28(1):58–81, 2014.
- [37] Yuxuan Du, Min-Hsiu Hsieh, Tongliang Liu, and Dacheng Tao. The expressive power of parameterized quantum circuits. *arXiv preprint arXiv:1810.11922*, 2018.
- [38] Nathan Killoran, Thomas R. Bromley, Juan Miguel Ar-razola, Maria Schuld, Nicolás Quesada, and Seth Lloyd. Continuous-variable quantum neural networks. *Phys. Rev. Research*, 1:033063, Oct 2019.
- [39] Brian Coyle, Daniel Mills, Vincent Danos, and Elham Kashefi. The born supremacy: Quantum advantage and training of an ising born machine. *arXiv preprint arXiv:1904.02214*, 2019.
- [40] Tameem Albash and Daniel A. Lidar. Adiabatic quantum computation. *Rev. Mod. Phys.*, 90:015002, Jan 2018.
- [41] LLC Gurobi Optimization. Gurobi optimizer reference manual, 2020.
- [42] M. Powell. A view of algorithms for optimization without derivatives. *Mathematics TODAY*, 43, 01 2007.
- [43] Kevin J. Sung, Matthew P. Harrigan, Nicholas C. Rubin, Zhang Jiang, Ryan Babbush, and Jarrod R. McClean. An exploration of practical optimizers for variational quantum algorithms on superconducting qubit processors. *arXiv preprint arXiv:2005.11011*, 2020.
- [44] Wim Lavrijsen, Ana Tudor, Juliane Mller, Costin Iancu, and Wibe de Jong. Classical optimizers for noisy intermediate-scale quantum devices. *arXiv preprint arXiv:2004.03004*, 2020.
- [45] M. Cerezo, Akira Sone, Tyler Volkoff, Lukasz Cincio, and Patrick J. Coles. Cost-function-dependent barren plateaus in shallow quantum neural networks. *arXiv preprint arXiv:2001.00550*, 2020.
- [46] The distribution function encoded in Eq. (4) is analogous to the trivial case of having a restricted Boltzmann machine with n_c visible nodes and no hidden layers. We also note that the expressive power of $|\psi_1(\vec{\theta})\rangle$ can be fully captured within the complete encoding scheme by using only a single layer of $R_y(\theta_i)$ rotations applied to each qubit. Studying the minimal encoding scheme is therefore akin to examining the amount of resources required to map the simplest quantum circuit of n_c qubits onto an exponentially narrower circuit.